Superposition of the uncertainties in acoustic responses and the robust design of active control systems

Stephen J. Elliott,[1] Jin Zhang,[1] Chung Kwan Lai,[1] and Jordan Cheer[1]

Institute of Sound and Vibration Research, University of Southampton SO17 1BJ, United Kingdom[a]

The use of virtual sensing allows the frequency range of a local active noise control system at a listener's ears to be extended beyond what is possible when only controlling at remote physical sensors, particularly if head tracking is also used to determine the position of the virtual sensors. As the frequency range is extended, however, the uncertainties in the acoustic responses become more significant and the design of multichannel adaptive controllers that are robustly stable to these uncertainties becomes more important. In order to fully characterise the uncertainties due to the combination of all the possible changes in the acoustic environment a very large number of measurements would, in principle, need to be taken. For uncertainties due to the simultaneous change in position of several objects within the acoustic environment, however, it is shown that the uncertainties can be accurately predicted by the superposition of the uncertainties due to the change in position of the objects individually. This allows the uncertainty due to the change in position of a number of objects to be rapidly evaluated from a limited number of experiments and considerably simplifies the controller design process, which is illustrated here for an active headrest system using two different virtual sensing techniques.

Keywords: Active control Additive uncertainty Robust design Virtual sensing

[a]jz1a19@soton.ac.uk

I. INTRODUCTION

Local active sound control, close to a listener's ear, has the potential to work up to a higher frequency than global active sound control systems, which aim to reduce the sound throughout an enclosure[1]. In particular, secondary loudspeakers incorporated into a headrest can be used for local active control at the ears of a seated listener[2,3]. The spatial extent of the zone of quiet generated around an error microphone whose output is cancelled by such a local active control system is of the order of 1/10 of an acoustic wavelength[4,5]. At higher frequencies, it is thus important to control the sound pressure close to the listener's ear, which can be difficult if physical error microphones are used. Using some assumptions about the nature of the sound field to be controlled, virtual sensing techniques enable the pressure at virtual error microphone positions, close to the listener's ears, to be estimated from the output of a number of remote monitoring microphones, without the use of physical microphone at listener's ears[6–9].

Using head tracking technology, the coordinates of two virtual error microphones can also be updated to always ensure control at the positions of a listener's ears[6]. It has been shown that under favourable conditions, such as system can achieve significant attenuation in the sound at the listener's ears at frequencies up to at least 1 kHz[10]. As well as needing to make assumptions about the nature of the sound field to be controlled, an adaptive local control system also requires an estimate of the plant responses, from the secondary loudspeakers to the monitoring microphones and the virtual error microphones. Both the primary sound field and the plant responses are subject to uncertainties in practical environments and it is important that the stability and performance of the local control system is robust to these uncertainties.

One important application of such a local active headrest system is in the control of mid-frequency road noise in vehicles, since it is known that global active control systems only work well up to about 300 Hz in this application[11,12]. Assuming that the position of the head can be accurately tracked, the main sources of uncertainty in the acoustic responses are due to changes in the positions of the seats or other passengers within the vehicle. One way of designing the controller in this case is to assume that the uncertainty is unstructured and that its magnitude is less than some upper bound[13,14]. Since the phase information and the interdependence between the uncertainties in the individual frequency responses is then lost, a controller designed to be robust to such uncertainty can be very conservative and its performance will not be as good as one designed to be robust only to the specific kind of uncertainties found in practice. It would, in principle, be necessary to measure all possible combinations of these perturbations that give rise to these uncertainties in order to have the data needed to design a controller that was robust to the all conditions of the possible uncertainties that could be encountered. Making the conservative assumption that there are 10 such individual perturbations in the sound field, for example, there would be 10 cases in which only one perturbation was present, 45 cases for the combination of any two perturbations and 120 cases for the combination of three perturbations, for example, as shown in Table I. Adding up all the different possibilities for the number of perturbations, it is clear that over 1000 experiments with different vehicle configurations would, in principle, need to be performed to capture all possibilities.

In this paper it is shown how the uncertainty associated with a number of these perturbations occurring simultaneously can be accurately approximated by the superposition of the uncertainties associated with each perturbation occurring individually. Following the example, it would only be necessary to undertake 10 measurements of the acoustic responses subject to the individual uncertainties, and then the uncertainties associated with all of the combinations of these perturbations could be calculated offline. In practice, this technique could be used to efficiently identify the combinations of uncertainty that would have the greatest effect on the stability and performance of an adaptive multichannel active control system, and hence enable the design of a control system that is robust to the worst case uncertainty that it will encounter.

Sec. II of this paper describes a series of experiments in which the acoustic responses for a headrest-based active control system were measured in a vehicle under various conditions. The uncertainty in the frequency responses due to two changes occurring simultaneously in the vehicle is then compared with those calculated by superposing the uncertainties due to the individual changes. In Sec. III, a time domain interpretation is used to help understand the success of this superposition of uncertainties and also illustrate its limitations. This also shows how computational methods could also be used to further reduce the number of experiments necessary to calculate the worst-case uncertainty. The design of adaptive active feedforward control systems that are robust to such a worst-case uncertainty is illustrated in Sec. IV, using two different virtual sensing strategies, before some overall conclusions are drawn in Sec. V.

II. ESTIMATION OF THE UNCERTAINTY IN THE FREQUENCY DOMAIN BY SUPERPOSITION

Fig. 1(a) illustrates the active control system used for the measurements when installed on the seat headrest in a medium-sized car[15]. The two secondary loudspeakers are denoted L1 and L2 and the physical monitoring microphones, used to estimate the pressure at the virtual error microphones, are denoted M1 to M4. Fig. 1(b) then shows the position of a dummy head in the driver's position, with microphones denoted E1 and E2 in the ears, which can be used as the error sensors during the identification, or training, stage of the active control system design. The left hand front seat is designated Seat 1, the right hand front seat is Seat 2 and the rear left and right hand seats are designated as Seats 3 and 4, as shown in Fig. 1(c). Measurements of the responses between the loudspeakers and microphones were conducted in the vehicle car cabin with 10 different uncertainties as listed in Table II.

Fig. 2 shows the magnitude and phase of the frequency response measured from one of the secondary loudspeakers, L2, to one of the monitoring microphones, M1, under four different conditions. These conditions include the nominal one, with the seats in their normal positions, one with Seat 2 being moved forward only, one with the back of Seat 3 being lowered only and finally with both Seat 2 moved forward and Seat 3 back lowered at the same time. The frequency response of the relatively small secondary loudspeakers falls off sharply below about 100 Hz, so that the measured responses are very small and noisy in this frequency region. At higher frequencies, differences of up to 7 dB in magnitude and

40° in phase can still be seen between the various measurements of the frequency response, with the variations generally becoming larger at higher frequencies.

Assuming that the complex frequency response under nominal conditions is denoted $\mathbf{G}_0(j\omega)$, the frequency responses measured with two individual perturbations in the vehicle can be written as

$$\mathbf{G}_1(j\omega) = \mathbf{G}_0(j\omega) + \Delta\mathbf{G}_1(j\omega), \tag{1}$$

$$\mathbf{G}_2(j\omega) = \mathbf{G}_0(j\omega) + \Delta\mathbf{G}_2(j\omega), \tag{2}$$

where $\Delta\mathbf{G}_1(j\omega)$ and $\Delta\mathbf{G}_2(j\omega)$ are the frequency responses of the additive uncertainties in these two cases. If both of these perturbations occur simultaneously, we can write the frequency response as

$$\mathbf{G}_{1,2}(j\omega) = \mathbf{G}_0(j\omega) + \Delta\mathbf{G}_{1,2}(j\omega) \tag{3}$$

If this uncertainty were to be estimated from the superposition of the uncertainties due to the two individual perturbations, this can be written as

$$\Delta\hat{\mathbf{G}}_{1,2}(j\omega) = \Delta\mathbf{G}_1(j\omega) + \Delta\mathbf{G}_2(j\omega) \tag{4}$$

Fig. 3 shows a comparison between the measured and the estimated uncertainties in the responses shown in Fig. 2 when both Seats 2 and 3 are moved, corresponding to $\mathbf{G}_{1,2}(j\omega)$ and $\Delta\hat{\mathbf{G}}_{1,2}(j\omega)$ above. It can be seen that there is remarkably good agreement, in both magnitude and phase, between the uncertainties due to the two perturbations occurring together and that calculated from the superposition of the two perturbations occurring in isolation. The physical reasons for this similarity will be explored in the following section, but to further illustrate the accuracy of this superposition, Fig. 4 shows the measured response between the secondary source L2 and the physical error microphone E1, in the dummy head, under two other conditions, where Seat 2 was moved back and a dummy person was positioned in Seat 3. In this figure, the maximum change in the response is up to 10 dB in magnitude and 30 degrees, except for the phase change at around 700 Hz. Fig. 5 shows the comparison between the measured uncertainties and that calculated by the superposition of the uncertainties when the two perturbations in Fig. 4 are applied. Again, good agreement in the combined uncertainty is observed. The frequency response of the uncertainties are relatively noisy compared with the individual frequency responses, since they represent the small difference between two large individual responses, each of which has some random measurement errors. Similar results are observed for other combinations of the uncertainties in the responses from the secondary loudspeakers to the monitoring and error microphones.

III. INTERPRETATION OF THE UNCERTAINTIES IN THE TIME DOMAIN

Although, from a frequency domain perspective, there does not appear to be any obvious reason for the success in predicting the uncertainty using superposition, this can be understood more clearly in the time domain. Fig. 6 shows the inverse Fourier transforms of the frequency responses shown in Fig. 2, i.e. the impulse responses, from the secondary source L2 to the monitoring microphone M1, under the four different conditions used in Fig. 2. It is clear that the responses before about 4 ms are very similar in all cases, since this corresponds to the direct field due to propagation between the loudspeaker and the microphone as if the seat were under anechoic conditions with no other reflections. There are clear differences in the later response, however, since these are affected by reflections due to the positions of the seats in the vehicle. These differences become greater in the final part of the impulse responses, which are due to multiple reflections.

Taking the inverse Fourier transforms of Eqs. (1) and (2) we can write the impulse responses due to the individual perturbations as

$$\mathbf{g}_1(t) = \mathbf{g}_0(t) + \Delta\mathbf{g}_1(t), \tag{5}$$

$$\mathbf{g}_2(t) = \mathbf{g}_0(t) + \Delta\mathbf{g}_2(t), \tag{6}$$

where $\mathbf{g}_0(t)$ is the impulse response under nominal conditions and $\Delta\mathbf{g}_1(t)$ and $\Delta\mathbf{g}_2(t)$ are the time domain uncertainties in the plant response. We can similarly expressed the measured and estimated impulse responses due to both perturbations, as in Eqs. (3) and (4), as

$$\mathbf{g}_{1,2}(t) = \mathbf{g}_0(t) + \Delta\mathbf{g}_{1,2}(t), \tag{7}$$

$$\Delta\hat{\mathbf{g}}_{1,2}(t) = \Delta\mathbf{g}_1(t) + \Delta\mathbf{g}_2(t), \tag{8}$$

Fig. 7 shows the individual uncertainties in the time domain and Fig. 8 shows a time domain comparison between the estimation of the uncertainty using the superposition of the individual uncertainties and that measured with these two perturbations acting together, calculated from the results in Fig. 6.

Since the direct field is almost unaffected by the change in the seat positions, the impulse responses of the uncertainties in Fig. 7 are very small before about 4 ms. The changes in the responses due to the initial reflections are large compared to the changes in the later part of the response, which are due to multiple reflections . The impulse response of the measured uncertainty due to the movement of the two seats and the estimate of this uncertainty, from the superposition of the uncertainty due to each of the seats being moved alone, in

Fig. 8, are very similar up to about 12 ms, since the initial reflections are well predicted by superposition. The prediction becomes less accurate with time, however, due to the multiple reflections, which eventually generates a reverberant field. The accuracy of the superposition of the additive uncertainty thus appears to be due to the additive nature of the early reflections.

This physical insight can be further understood from the simplified geometry illustration in Fig. 9, in which the direct and reflected acoustic paths from a loudspeaker to a microphone are shown in an anechoic environment with two reflecting objects. Fig. 9(a) shows the assumed geometry and the corresponding idealised impulse response, showing the direct propagation path from the loudspeaker to the microphone, the first reflection from object 1, the first reflection from object 2, and finally the multiple reflections from both objects. Fig. 9(b) shows the change in the impulse response when object 1 is moved closer to the loudspeaker, so that the first reflection peak is now earlier and the dip indicates the absence of the original first refection. Similarly Fig. 9(c) shows the change in the impulse response when object 2 is moved further away from the loudspeaker, so that the first reflection peak now occurs later and the initial dip is due to the absence of the original first reflection. The part of the impulse response due to the direct path is unaltered in the geometries of Figs. 9(b) and 9(c), so there is no change in the impulse response earlier than the first reflection. Also, since the magnitude of the early reflections is large compared to that due to multiple reflections later on, they play a more significant role in the changes in the impulse responses and hence the uncertainty. Finally, Fig. 9(d) shows the change in the impulse responses when both object 1 is brought closer and object 2 is moved further from the loudspeaker, and in this case there is both a peak due to the earlier refection from object 1 and a peak due to the absence of the later reflection from object 2. It is clear that the overall change in the impulse response due to the first reflections is exactly equal to the sum of the two individual changes shown in Figs. 9(b) and 9(c), although the later multiple reflections will change somewhat. So, the success of the superposition of the uncertainties in the frequency domain is mainly due to the superposition of the effects of the early reflections, which form the dominant part of the uncertainty responses when considered in the time domain.

Although we have only considered the uncertainty in the response from one loudspeaker to one microphone above, in a multichannel system it is convenient to arrange the responses from each loudspeaker to each microphone in a matrix of plant responses. The matrix of plant frequency responses measured under a perturbed condition could then be written as

$$\mathbf{G}_1(j\omega) = \mathbf{G}_0(j\omega) + \Delta\mathbf{G}_{1\mathrm{e}}(j\omega) + \Delta\mathbf{G}_{1\mathrm{r}}(j\omega) \tag{9}$$

where $\mathbf{G}_0(j\omega)$ is the matrix of nominal responses, with no perturbations, $\mathbf{G}_{1\mathrm{e}}(j\omega)$ is the matrix of uncertainties due to changes in the early reflections and $\mathbf{G}_{1\mathrm{r}}(j\omega)$ is that due to changes in the more reverberant field. As noted above, the magnitudes of the elements in $\mathbf{G}_{1\mathrm{e}}(j\omega)$ will be considerably greater than those in $\mathbf{G}_{1\mathrm{r}}(j\omega)$. It is also noteworthy, however, that the form of the individual responses in the elements of the matrix $\mathbf{G}_{1\mathrm{e}}(j\omega)$ will all be related and determined by the geometry of the changes within the enclosure. In the terms used for robust multichannel control systems, this matrix of uncertainties is described as being structured[13,14]. In contrast, the smaller terms in $\mathbf{G}_{1\mathrm{r}}(j\omega)$ will be related to one another in a more complicated way and in a completely reverberant field will be uncorrelated. In terms of robust multichannel control, this form of uncertainty is described as being unstructured.

As well as being able to directly measure $\mathbf{G}_{1\mathrm{e}}(j\omega)$ due to a number of individual changes within the environment, it would also be possible to estimate the terms in this matrix from a simple acoustic model involving reflections under anechoic conditions, in a multichannel version of the arrangement illustrated in Fig. 9. Similarly, the amplitudes of the multiple reflections could be modelled to estimate the magnitude of the elements in $\mathbf{G}_{1\mathrm{r}}(j\omega)$. In this way, a limited number of experimental measurements could be enhanced, using a simple model, to estimate the uncertainty associated with the movement of many objects within the acoustic environment.

IV. ROBUST STABILITY IN CONTROL SYSTEMS USING VIRTUAL SENSORS

Virtual sensing systems are important in active noise control, since they allow the upper frequency of control to be increased, as mentioned in the introduction, but their stability then becomes more sensitive to uncertainties in the environment. In this section we illustrate how the superposition of uncertainties measured in a vehicle can be used to predict the stability of active control systems using various virtual sensing strategies and also help to tune these strategies to be robust to the whole range of operating conditions that will be encountered in practice. Two different virtual sensing strategies that are widely used in active sound control systems will be considered: the remote microphone, RM, method[16,17] and the additional filter, AF, method[18]. The block diagrams of feedforward control systems using these two remote sensing methods are shown in Fig. 10, in which $\boldsymbol{x}$ is a vector of reference signals and $\boldsymbol{W}$ if the matrix of responses of the multichannel adaptive controller.

In both methods the outputs of the physical monitoring microphones, $\mathbf{m}$, are the sum of the disturbances at these microphones, $\mathbf{d}_{\mathrm{m}}$, and contributions from the controller, $\mathbf{W}$, filtered by the physical plant response $\mathbf{G}_{\mathrm{m}}$. The analysis is performed in the frequency domain but the explicit dependence in frequency is suppressed for notational convenience. For the remote microphone method, shown in Fig. 10(a), the signals at the virtual error microphones are explicitly estimated, as $\hat{\mathbf{e}}$. This is achieved by first using an estimate of the plant response to the monitoring microphones, $\hat{\mathbf{G}}_{\mathrm{m}}$ measured during an identification phase, to cancel the effect of the controller to give an estimate of the disturbance at the monitoring microphones, $\mathbf{d}_{\mathrm{m}}$, and then using an "observation filter", $\mathbf{O}$, to predict the disturbances at the virtual error sensors, $\mathbf{d}_{\mathrm{e}}$, from the estimated disturbance at the monitoring microphones, $\hat{\mathbf{d}}_{\mathrm{m}}$. Finally, the identified estimate of the plant response at the virtual microphones, $\hat{\mathbf{G}}_{\mathrm{e}}$, is used to calculate the contribution due to the control signals at this microphone, which is added to $\hat{\mathbf{d}}_{\mathrm{e}}$ to give the estimated signal at the error microphones, $\hat{\mathbf{e}}$. The estimated virtual error signals are then minimise using the FxLMS algorithm, with the reference signals filtered by $\hat{\mathbf{G}}_{\mathrm{e}}$. It can be shown[10,19] that the multichannel adaptive control system using the RM method is stable provided the following condition is met at all frequencies present in the reference signals

$$\mathrm{Re}\left(\mathrm{eig}\left[\hat{\mathbf{G}}_{\mathrm{e}}^{\mathrm{H}}\hat{\mathbf{G}}_{\mathrm{e}}+\hat{\mathbf{G}}_{\mathrm{e}}^{\mathrm{H}}\mathbf{O}\left(\mathbf{G}_{\mathrm{m}}-\hat{\mathbf{G}}_{\mathrm{m}}\right)\right]\right)>0, \tag{10}$$

where the superscript $(\cdot)^{\mathrm{H}}$ denotes the Hermitian, complex conjugate, transpose of the matrix. The design of the observation filter, $\mathbf{O}$, involves the regularised inversion of the power spectral density matrix of disturbance at the monitoring microphones, $\mathbf{S}_{\mathbf{d}_{\mathrm{m}}\mathbf{d}_{\mathrm{m}}}$[19],

$$\mathbf{O}_{\mathrm{Opt}}=\mathbf{S}_{\mathbf{d}_{\mathrm{m}}\mathbf{d}_{\mathrm{e}}}\left[\mathbf{S}_{\mathbf{d}_{\mathrm{m}}\mathbf{d}_{\mathrm{m}}}+\beta\mathbf{I}\right]^{-1}. \tag{11}$$

The choice of regularisation parameter, β, has been shown to be a trade-off between obtaining a good estimate of $\hat{\mathbf{e}}$ and reducing the condition number of the matrix being inverted, which determines the robustness of the virtual sensing method. If the elements in the observation filter matrix have large magnitudes, due to ill-conditioning in Eq. (11), it can be seen from Eq. (10) that this magnifies the effect of any difference between $\mathbf{G}_{\mathrm{m}}$ and $\hat{\mathbf{G}}_{\mathrm{m}}$, and so makes the stability more sensitive to such differences.

Fig. 10(b) shows the other widely used virtual sensing algorithm, the additional filter method. In this method the outputs of the monitoring microphones are compared with those of an "additional filter", $\mathbf{H}$, which has been previously designed during an identification phase of the algorithm to be equal to the response between the reference signals and the monitoring microphones when the virtual error sensors are perfectly controlled. The difference between the two signals, $\boldsymbol{\epsilon}$, is thus a measure of how well the system is controlling the virtual error sensors, and the mean square value of this signal is minimised using the FxLMS algorithm. This updates the controller, $\mathbf{W}$, using the product of the measured difference signal, $\boldsymbol{\epsilon}$, and the reference signal, $\mathbf{x}$, filtered by the internal estimate of the plant response to the monitoring microphones, $\hat{\mathbf{G}}_{\mathrm{m}}$.

The control system using the AF method thus reduces to a more conventional multichannel adaptive control system, which is stable provided that the following condition is met at all frequencies present in the reference signals[14]

$$\mathrm{Re}\left(\mathrm{eig}\left[\hat{\mathbf{G}}_{\mathrm{m}}^{\mathrm{H}}\mathbf{G}_{\mathrm{m}}\right]\right) > 0, \tag{12}$$

The stability condition for adaptive controllers using either the AF or the RM methods of virtual sensing thus depend, in rather different ways, on the difference between the matrix of physical plant responses between the secondary sources and the monitoring microphones, $\mathbf{G}_{\mathrm{m}}$, and the internal estimate of this matrix that is used within the adaptive algorithm, $\hat{\mathbf{G}}_{\mathrm{m}}$. If there is no difference between $\mathbf{G}_{\mathrm{m}}$ and $\hat{\mathbf{G}}_{\mathrm{m}}$, then both methods are stable since the satbility conditions in both Eqs. (10) and (12) will be satisfied.

A series of simulations has being conducted, using the plant responses measured for the 10 perturbations in the vehicle arrangement described above, to test the stability conditions for these two algorithms under different operating conditions. It has been assumed that the internal estimate of the plant response from the secondary loudspeakers to the monitoring microphones, $\hat{\mathbf{G}}_{\mathrm{m}}$, is given by the nominal responses measured in the vehicle, with no perturbations. The various physical plant responses, $\mathbf{G}_{\mathrm{m}}$, are then assumed to include different combinations of the measured perturbations, as calculated using the superposition method.

Fig. 11(a) shows the set of 10 plots of the real parts of the smallest eigenvalues in Eq. (10) as a function of frequency, for the RM method, with each individual measured perturbation in $\mathbf{G}_{\mathrm{m}}$. Since the real parts of these eigenvalues under all of these conditions are always positive, the control system is predicted to remain stable for all cases of a single perturbation. Fig. 11(b) shows the results in the case where the 45 combinations of two perturbations are included, as calculated by superposition of the uncertainties, together with the 10 individual ones and since the real parts of all the eigenvalues are again positive, the control system is predicted to be stable for all pairs of perturbations occurring simultaneously. When the 120 possible combinations of three perturbations are also included together with the cases above, however, as in Fig. 11(c), the smallest eigenvalue in some cases becomes negative at particular frequencies, at around 400 Hz and 900 Hz for example, indicating that the control system would be unstable with this combination of perturbations. It is then possible to track down which specific combinations of uncertainty cause instabilities at which frequency. Finally, Fig. 11(d) shows the set of cases when all 1024 combinations of all the perturbations are exhaustively considered. In this case the instabilities are predicted to occur at similar frequencies to those in Fig. 11(c), but at 400 Hz for example, the probability of an instability increases from about 1% with three perturbations to about 20% with all possible perturbations. The simulations have been performed with no regularisation in the design of the observation filter, although it is known that increasing this regularisation factor will improve the robustness of the controller. The calculation of these results provide a principled method of choosing the regularisation factor at each frequency in order to ensure stable operation over all operating conditions, whilst maintaining the best possible performance.

Fig. 12 shows the corresponding results for the real parts of the eigenvalues that determine the stability condition for the AF method, in Eq. (12). In this case it is clear that the real parts of the eigenvalues remain positive at all frequencies, for all possible combinations of the measured uncertainty. No additional steps thus need to be taken in this case to ensure the robust stability of an adaptive controller using the AF method. If the magnitudes of the uncertainties were larger, so that additional robustness was required, a leakage factor could be selectively introduced into the adaptive algorithm at the frequencies of potential instability to guarantee stability. Although it is beyond the scope of the present paper, it is also important to consider the robust performance, in addition to the robust stability, in the comparison of control systems using different virtual sensing methods. Whereas the AF method is robust to changes in the plant responses, its performance is found to be rather sensitive to changes in the properties of the reference signals, and so the best choice of virtual sensing method depends very much on the particular application.

V. CONCLUSIONS

As the frequency range of active sound control systems is extended, using virtual sensing methods for example, the effect of uncertainties in the acoustic responses on the stability of the control system becomes more significant. It is important when designing control systems that are robustly stable that all possible combinations of operating condition are accounted for. To fully characterise the uncertainties due to all possible changes in the acoustic environment, however, a very large number of measurements would, in principle, need to be taken. For uncertainties due to the simultaneous change in position of several objects within the acoustic environment it is shown that the uncertainties can be accurately predicted by the superposition of the uncertainties due to the change in the positions of the objects individually.

This is initially illustrated using a set of measurements taken for an active headrest system in a vehicle under a variety of conditions. A time-domain explanation for the superposition of the measured uncertainties is put forward, based on the changes in the early reflections. The superposition property allows the uncertainty due to the movement of a number of objects to be rapidly evaluated from a limited number of experiments when the objects are moved individually, which can considerably simplify the controller design process. This is illustrated for the active headrest system using an adaptive feedforward control system with two different virtual sensing techniques, the remote microphone method and the additional filter method. The stability with the additional filter method is found to be inherently robust to the range of changes calculated from measurements in a vehicle, but that of the remote microphone method without regularisation of the observation filter is not. The remote microphone method does, however, have other advantages over the additional filter method, such as good performance when the characteristics of the reference signals are subject to change. The stability condition calculated under all of the different operating cases, synthesised using uncertainty superposition, allows the parameters of the adaptive algorithm to be tuned at specific problematic frequencies to ensure robust stability, allowing the performance at other frequencies to be preserved.

The superposition of additive uncertainties would not be valid for all systems. For example if a mechanical system were characterised by lightly damped and isolated modes, the effect of an increase in stiffness or a decrease in mass might almost cancel each other out if applied simultaneously, whereas the individual additive uncertainties would not cancel. The superposition of uncertainties has been shown above to be a reasonable approximation for systems governed by wave propagation and reflections, however, and so should be generalizable to other systems where uncertainty in the acoustic responses affects the system performance, such as in transducer array systems for audio reproduction and in acoustic sensing.

ACKNOWLEDGEMENT

The authors gratefully acknowledge the support of the UK Engineering and Physical Sciences Research Council (EPSRC) through the DigiTwin project (grant EP/R006768/1).

REFERENCES

[1]P. A. Nelson and S. J. Elliott, *Active Control of Sound* (Academic press, 1992).

[2]H. F. Olson and E. G. May, “Electronic sound absorber,” J. Acoust. Soc. Am. **25**(6), 1130–1136 (1953).

[3]B. Rafaely and S. J. Elliott, “H_2 / H_∞ active control of sound in a headrest: design and implementation,” IEEE Transactions on control systems technology **7**(1), 79–84 (1999).

[4]S. J. Elliott, P. Joseph, A. J. Bullmore, and P. A. Nelson, “Active cancellation at a point in a pure tone diffuse sound field,” J. Sound Vib. **120**(1), 183–189 (1988).

[5]J. Garcia-Bonito, S. J. Elliott, and C. C. Boucher, “Generation of zones of quiet using a virtual microphone arrangement,” J. Acoust. Soc. Am. **101**(6), 3498–3516 (1997).

[6]D. Moreau, B. Cazzolato, A. Zander, and C. Petersen, “A review of virtual sensing algorithms for active noise control,” Algorithms **1**(2), 69–99 (2008).

[7]C. Shi, R. Xie, N. Jiang, H. Li, and Y. Kajikawa, “Selective virtual sensing technique for multi-channel feedforward active noise control systems,” in *ICASSP 2019-2019 IEEE International Conference on Acoustics, Speech and Signal Processing (ICASSP)*, IEEE (2019), pp. 8489–8493.

[8]D. P. Das, D. J. Moreau, and B. Cazzolato, “Performance evaluation of an active headrest using the remote microphone technique,” Proceedings of Acoustics 2011 2–4 (2011).

[9]A. Siswanto, C. Chang, and S. M. Kuo, “Active noise control for headrests,” in *2015 Asia-Pacific Signal and Information Processing Association Annual Summit and Conference (APSIPA)*, IEEE (2015), pp. 688–692.

[10]S. J. Elliott, W. Jung, and J. Cheer, "Head tracking extends local active control of broadband sound to higher frequencies," Scientific reports **8**(1), 1–7 (2018).

[11]T. J. Sutton, S. J. Elliott, A. M. McDonald, and T. J. Saunders, "Active control of road noise inside vehicles," Noise Control Engineering Journal **42**(4), 137–147 (1994).

[12]Hyundai, "Hyundai motor group develops world's first road active noise control technology," (2020) https://www.hyundai.co.nz/hyundai-road-active-noise-control-technology (Last viewed June 14, 2020).

[13]S. J. Elliott, *Signal processing for active control* (Elsevier, 2000).

[14]S. Skogestad and I. Postlethwaite, *Multivariable feedback control: analysis and design*, Vol. 2 (Wiley New York, 2007).

[15]S. J. Elliott, C. K. Lai, T. Vergez, and J. Cheer, "Robust stability and performance of local active control systems using virtual sensing," in *23rd International Congress on Acoustics*, Aachen, Germany (September 9–13, 2019), pp. 61–68.

[16]S. J. Elliott and J. Cheer, "Modeling local active sound control with remote sensors in spatially random pressure fields," J. Acoust. Soc. Am. **137**(4), 1936–1946 (2015).

[17]W. Jung, S. J. Elliott, and J. Cheer, "Local active control of road noise inside a vehicle," Mechanical Systems and Signal Processing **121**, 144–157 (2019).

[18]M. Pawelczyk, "Adaptive noise control algorithms for active headrest system," Control Engineering Practice **12**(9), 1101–1112 (2004).

[19]W. Jung, S. J. Elliott, and J. Cheer, "Combining the remote microphone technique with head-tracking for local active sound control," J. Acoust. Soc. Am. **142**(1), 298–307 (2017).

LIST OF TABLES

TABLE I. Number of combinations of cases for different numbers of perturbation

Number of perturbation	0	1	2	3	4	5	6	7	8	9	10	Total
Number of cases	1	10	45	120	210	252	210	120	45	10	1	1024

TABLE II. List of 10 perturbations conducted for the measurement in the test vehicle.

Perturbation type	
Seat 1 moved forward	Seat 4 back lowered
Seat 2 moved back	Dummy in Seat 2
Seat 2 moved forward	Dummy in Seat 3
Seat 2 back lowered	Box in front of Seat 1
Seat 3 back lowered	Box in front of Seat 2

LIST OF FIGURES

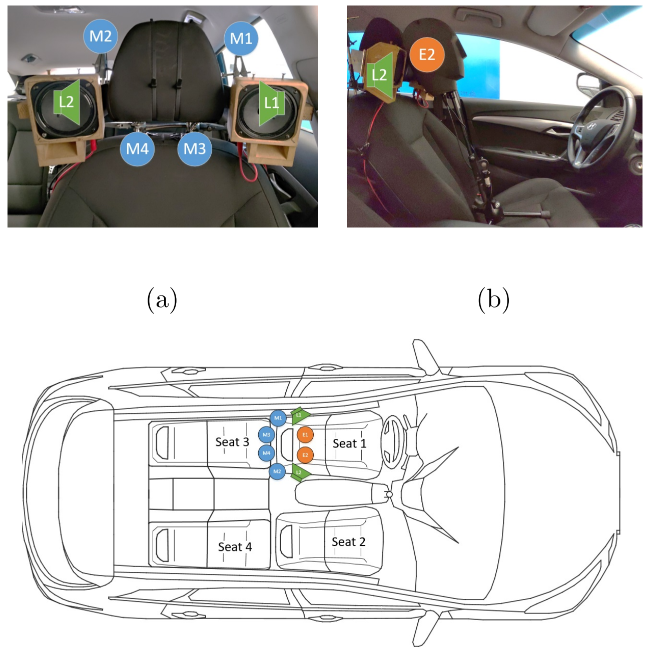

(c)

FIG. 1. The arrangement of the secondary loudspeakers, L1 and L2, in the headrest of the test vehicle, together with the monitoring microphones, M1 to M4, and the error microphones in the ears of the dummy head, E1 and E2. Front and side views of seat 1 are shown in (a) and (b), and a plan view of the whole vehicle, showing the numbering of the seats is shown in (c).

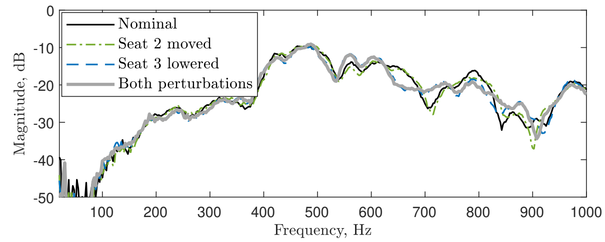

(a)

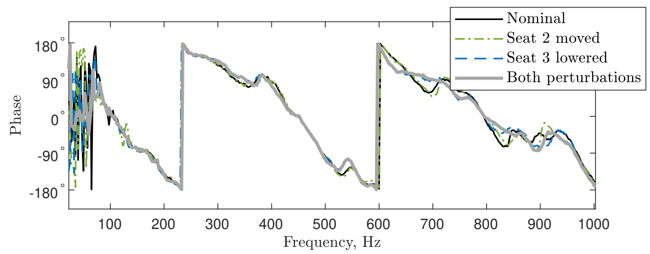

(b)

FIG. 2. Acoustic response from loudspeaker L2 to monitoring microphone M1, measured under nominal conditions and two conditions with individual perturbations, due to seat 2 being moved forward and the back of seat 3 being lowered, and then with both perturbations acting together.

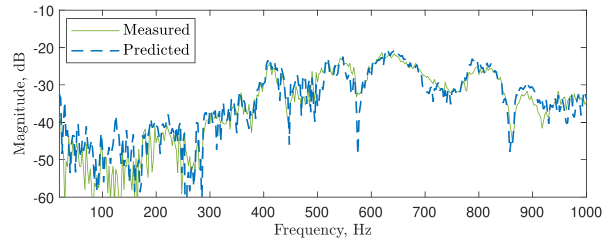

(a)

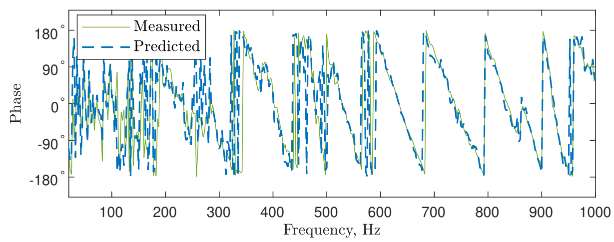

(b)

FIG. 3. Additive uncertainty, calculated from the results in Fig. 2, when measured with the two perturbation conditions acting together and when this is predicted from the sum of the additive uncertainties of two conditions separately.

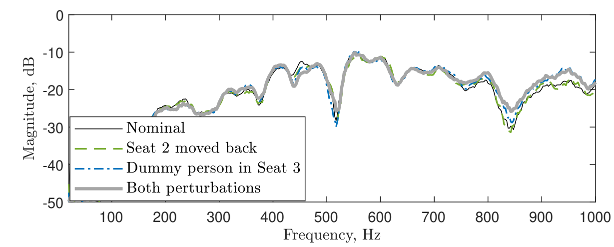

(a)

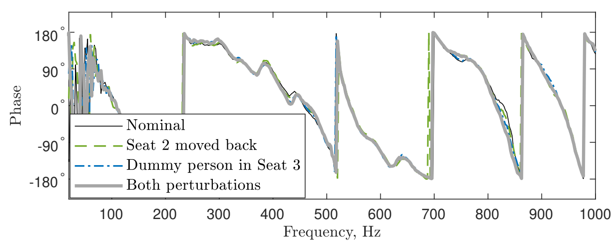

(b)

FIG. 4. Acoustic response from loudspeaker L2 to error microphone E1, measured under nominal conditions and two conditions with individual perturbations, due to Seat 2 being moved back and a dummy head and torso being placed in Seat 3, and then with both perturbations acting together.

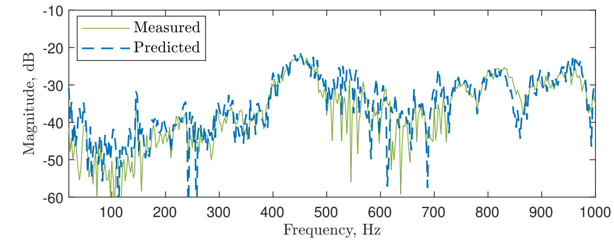

(a)

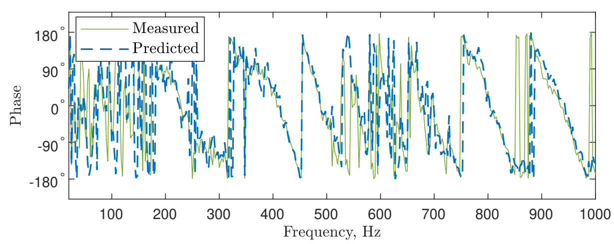

(b)

FIG. 5. Additive uncertainty, calculated from the results in Fig. 4, when measured with the two perturbation conditions acting together and when this is predicted from the sum of the additive uncertainties of two conditions separately.

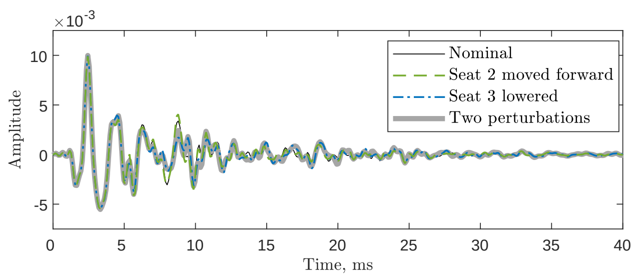

FIG. 6. Impulse response from loudspeaker L2 to monitoring microphone M1, measured under nominal conditions and two conditions with individual perturbations, due to Seat 2 being moved forward and Seat 3 being lowered, and then with both perturbations acting together.

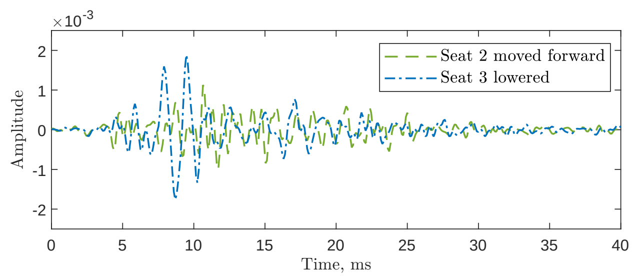

FIG. 7. Impulse response of the additive uncertainty, calculated from the results in Fig. 6, when measured with the two perturbation conditions acting separately.

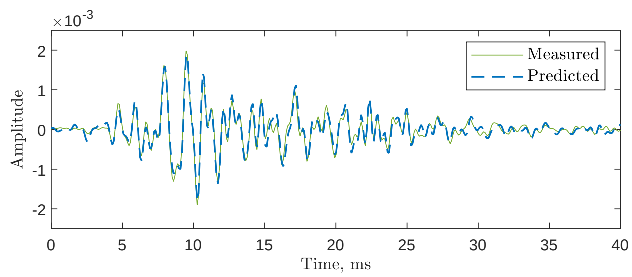

FIG. 8. Impulse response of the additive uncertainty, calculated from the results in Fig. 7, when measured with the two perturbation conditions acting together and when this is predicted from the sum of the additive uncertainties of two conditions separately.

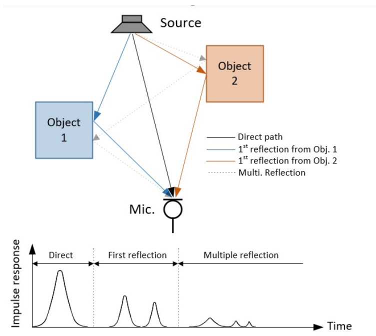

(a)

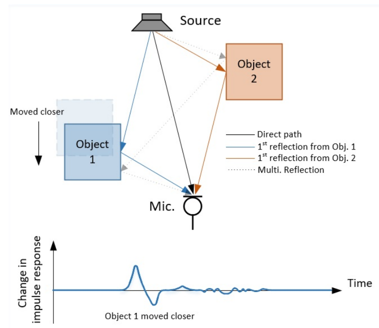

(b)

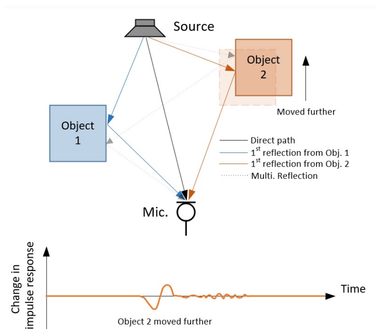

(c)

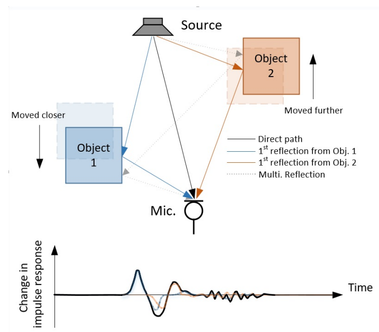

(d)

FIG. 9. Schematic to illustrate the change in the direct and reflected acoustic paths from a loudspeaker to a microphone in the change of the impulse responses in an anechoic environment with two reflecting objects.

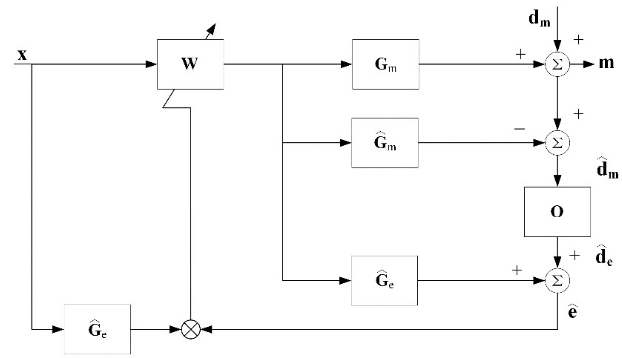

(a)

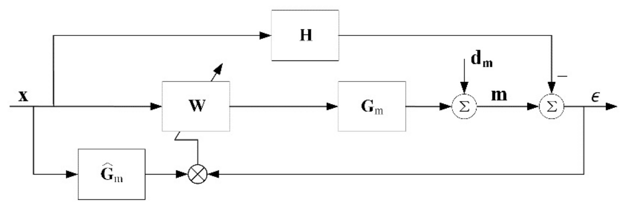

(b)

FIG. 10. Block diagrams of two virtual sensing methods for active noise control: (a) RM method, (b) AF method.

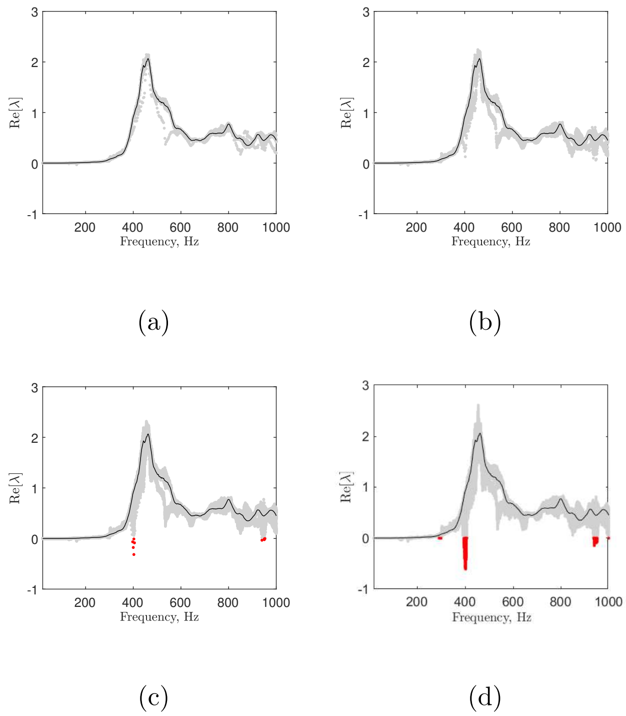

FIG. 11. The real parts of the smallest eigenvalue, shown as a cluster of points, for the stability of the RM method, when including up to 1, (a), 2, (b), 3 (c) and 10 (d) perturbations measured in the vehicle. The points coloured in red are those with negative eigenvalues. The eigenvalue spectrum under the nominal condition is shown by the solid black line.

(a)(b)

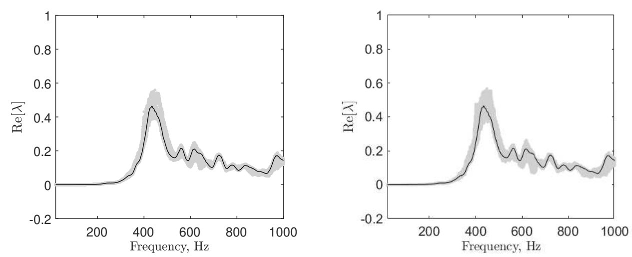

(c) (d)

FIG. 12. The real parts of the smallest eigenvalue, shown as a cluster of points, for the stability of the AF method, when including up to 1, (a), 2, (b), 3 (c) and 10 (d) perturbation(s) measured in the vehicle. The eigenvalue spectrum under the nominal condition is also shown as the solid black line.